Engineering Notes

Experimental Evaluation of Solid Propellant Rocket Motors under Acceleration Loads

JOHN G. HORTON II*
Thiokol Chemical Corporation, Elkton, Md.

INDUSTRY has been concerned with the effects of high acceleration loads on solid propellant rocket motors since the latter half of the 1950's. Possible influences of acceleration on the performance of a rocket motor include both ballistic and structural integrity changes, including excessive creep, cracking, or other changes in the grain configuration. Propellant-liner separation and associated side-burning may also cause erratic motor performance or failure. Surface area changes (grain deformation), ignition abnormalities, or burning rate variation may have adverse effects on the internal ballistics of a motor.

Specific studies of effects of acceleration forces on the burning characteristics of solid propellants were relatively limited before 1957. In the early 1960's, studies were made to specify the effects of high inertial loadings upon propellant combustion and motor stability. These investigations were classified as: 1) studies concerned with the effects of high-g forces on burning rate, and, 2) studies related to the determination of problems in the design and operation of conventional rocket motor systems.[1–4]

At its inception, the present program represented one of the first over-all investigations of the performance of sizable solid propellant motors subjected to high acceleration loads under centrifugal firing conditions. Its objective was to determine the effects of centrifuge-simulated acceleration forces on the ballistic performance and physical integrity of large solid propellant rocket motors. Eleven rocket motors (including one inert startup motor) were tested on a centrifuge under loads of 50- and 100-g accelerations, and five motors were static tested to determine a basis for ballistic comparison and evaluation. Of the sixteen motors manufactured, eight were cast with a cylindrical perforated (CP) grain and eight with a six-point star grain design (including one that was inert).

Experimental Approach

The over-all program approach involves the use of a well-characterized propellant in a reliable heavyweight test motor and the selection of a suitable testing facility. The Component Evaluation Laboratories were selected to perform the acceleration testing. The centrifuge unit was designed to provide accelerations as high as 150 g's to rocket motors of over 300 lb. It is composed of 1) a welded steel structural base anchored to a concrete pad, 2) the main boom constructed of two I beams at the end of which is mounted the test rocket motor, 3) a 260-hp diesel power unit, and, 4) test instrumentation composed of a probe bridgewire slip-ring oscillograph measuring circuit, a pressure and thrust strain gage unit, and an acceleration strain gage system.

The test motor was a modified Thiokol TE-243, heavyweight, carbon steel, 8-in. ballistic test motor. Motor and grain details are illustrated and tabulated in Fig. 1. The motor assembly consists of a steel case with an elliptical-shaped head end and a peripheral thrust skirt, a steel nozzle body, and a Speer-type 890S extruded electrographite nozzle throat insert. The nozzle assembly is joined to the motor case by a Marman coupling arrangement. The igniter and head end adapter are fastened to the motor body with Marman clamps. The dual squib pyrotechnic igniter was capable of withstanding the 100-g acceleration loads.

All units that were centrifuge tested had web burnout probes installed through the case wall with measurement pickups located at the interface between the liner and the propellant. Ten of these ionization (breakwire) probes were mounted in a straight line along the longitudinal axis of the motor (Figs. 1 and 2). Burning time as related to nozzle erosion, slump, or deformation of the grains during centrifuge testing was evaluated using burnout probe data.

These motors were designed to operate at a nominal average chamber pressure of 600 psi with a burning time of 5.2 sec. The thrust-time and pressure-time curves for the star design are essentially neutral ($P_{c\ max}/P_{av} = 1.05$), but the CP configuration provides a slightly progressive trace ($P_{c\ max}/P_{c\ initial} = 1.25$). The motors were bayonet cast using one batch of Thiokol PBAA propellant for each grain configuration. All motors were cast through the aft end and case-bonded using a compatible PBAA liner. Static tests, live motor nonfiring tests, and analysis of live motor centrifuge firing tests revealed no unbonding or grain separation.

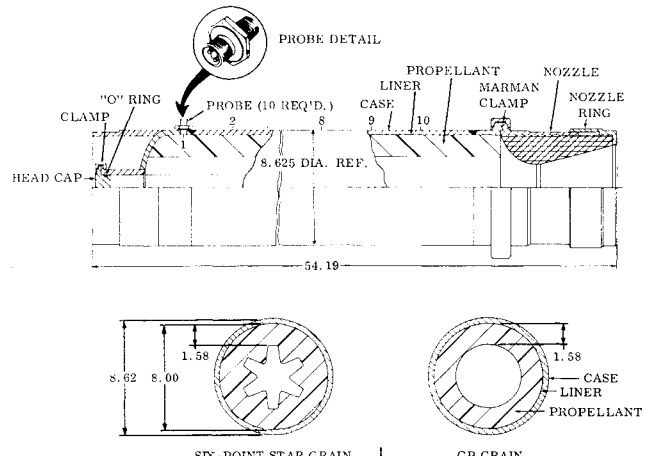

	SIX-POINT STAR GRAIN	CP GRAIN
Cross-sectional loading density, ℚ	77	63
Propellant weight, lb	100.0	81.3
Liner weight, lb	0.8	0.8
Inert parts wt., lb	178.2	177.9
Igniter wt., lb	1.0	1.0
Nozzle throat diam, in.	> 2	> 2
Nozzle exit diam, in.	> 6	> 5
Grain modulus, psi	585	548
Grain stress, psi	104	104
Grain strain, in./in.	0.254	0.271

Fig. 1 Modified TE-243 8-in. ballistic test motor components and grain configuration.

Presented as Preprint 64-133 at the AIAA Solid Propellant Rocket Conference, Palo Alto, Calif., January 29–31, 1964; revision received June 1, 1964. This program was conducted under Contract AF04(611)-8163 with the Air Force Rocket Propulsion Laboratory, Edwards Air Force Base, Calif. The author wishes to express his thanks to M. D. Rosenberg, H. W. Mulkins, W. G. Andrews, W. N. Rowe, and C. R. Huskey for their valuable assistance in the preparation of this paper.

* Program Manager, Elkton Division; now at Aberdeen Proving Grounds, Md. Member AIAA.

Table 1 Probe data summary on star- and CP-grain motors

Motor no.	g load	P_c, psia	Burning rate, in./sec	Probe numbers 1	2	3	4	5	6	7	8	9	10	Mid-mean av, in./sec
Star grain														
−8	0	593	0.317	4.85	5.09	...	...	5.13	5.00	...	...	4.85	5.02	4.99
−5	0	584	0.310	4.94	5.27	5.27	5.22	5.18	5.12	5.03	5.06	5.03	4.99	5.10
−9	50	624	0.297	4.51	5.03	5.13	5.24	5.36	5.33	5.40	6.36	5.36	6.68	5.32
−6	50	606	0.316	4.88	4.71	5.01	5.50	4.71	5.12	5.13	5.08	5.03	4.57	5.00
−4	100	608	0.300	5.17	5.55	5.62	5.70	5.61	5.07	5.16	5.21	5.14	5.07	5.27
−7	100	607	0.307	5.03	5.40	5.40	5.19	5.20	5.09	5.18	5.08	4.94	5.01	5.14
CP grain														
−1	0	570	0.302	5.24	...	5.36	...	5.31	5.27	5.17	5.23	5.15	5.20	5.24
−6	0	585	0.304	4.91	5.34	5.18	5.38	4.86	...	...	5.33	...	...	5.20
−5	50	588	0.311	4.88	5.09	5.37	5.19	5.20	5.35	5.32	5.34	5.30	5.41	5.08
−4	100	591	0.311	5.21	5.08	5.15	5.08	5.08	5.07	5.08	5.10	5.08	5.27	5.09
−3	100	611	0.318	5.01	5.03	5.06	5.24	4.87	4.89	4.95	4.96	4.96	4.87	4.97

Experimental Test and Discussion

A CP-grain motor containing an inert solid propellant grain having the same physical properties as the live motors was used for centrifuge startup and checkout of the acceleration technique. This motor was rotated for 5 min at 50 g's and 5 min at 100 g's before approval to test live motors was granted.

Five motors were then static tested to perfect the breakwire probe measuring technique and to act as a ballistic standard of comparison with the accelerated motor firings. Next, one motor of each grain design was accelerated at 50 g and 100 g for 1 min each to determine whether the acceleration would cause any residual effects on the motor grain. Full acceleration on the centrifuge was attained in a smooth and gradually accelerating manner. The lateral cross-axial acceleration did not exceed 5 g. Less than 2 g loss of acceleration was noted during the gear transmission shifting when approaching 100 g. At the end of these "live-no-fire" acceleration tests, x-ray, visual, and linear inspection showed no measurable effects.

The remaining eight motors, four star-point and four CP-grain configurations, were acceleration tested. Probes of all eight motors functioned satisfactorily, but the failure of test equipment during one test precluded the recording of probe data. The probe data were based on the time to interrupted current flow through the bridgewire; however, the very large variation in values indicated that the bridgewire in some cases was breaking prematurely. Consequently, the probe data were re-evaluated using the redundant measure of time to onization as a measure of web burnout. Therefore, all probe data are based on the time-to-current transmission due to ionization at the probe terminals.

Thrust-time data are not reported because of the difficulties encountered in the accurate measurement of thrust during centrifuging. The accuracy of this measurement was significantly decreased due to the necessity for correcting thrust gage readings to account for mass discharge during motor operation. Mass discharge was not monitored and estimations based upon instantaneous chamber pressure did not prove satisfactory. It is also possible that there were slight movements in the thrust acquisition fixtures which contributed to this difficulty. All other data were consistent with values obtained from the previous static firing control tests.

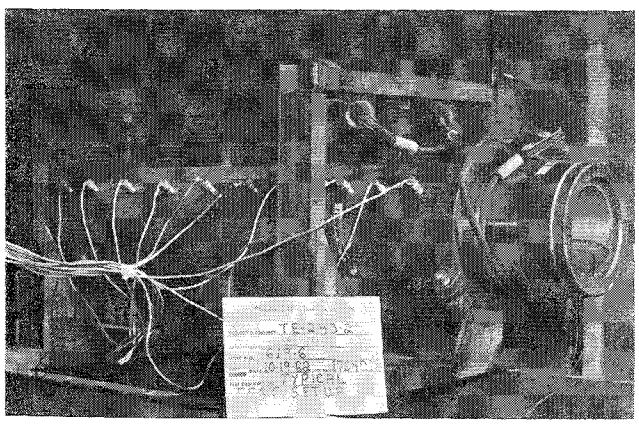

Fig. 2 Eight-inch ballistic test motor showing breakwire probe terminals before static test.

Discussion of Results

Burning-rate analysis

Reported burning rate: This is defined as the quotient of the propellant web thickness divided by the burning time at 10% of maximum chamber pressure to time of propellant web burnout. Analysis of data indicate that all test points were within the burning-rate limits as defined for this motor. The close grouping of the data together with their distribution within the group and the limited number of test points for each test condition tends to preclude a statistical analysis. Burning rate vs $P_{0_{av}}$, characteristics showed no abnormalities.

Ionization probe data: The time web burnout was indicated by ionization of the 10 breakwire probes. The web thickness was divided by this burning time to define the propellant burning rate. The limited number of test points for each test condition and the grouping of these data would not support statistical analysis. X-ray examination of the motors before test firing showed no propellant voids affecting the probe data. There are no conclusive probe data indicating differences in propellant burning rate or burning characteristics between the control motors and centrifuged motors. Table 1 summarizes the probe data, mid-mean average burnout time, and resulting burning rate.

Conclusions

There was no change in propellant burning rate nor any other significant trend, due to high accelerations; however, this conclusion is limited by 1) the use of a PBAA propellant between ambient test temperatures of 65° to 85°F, and 2) experimental motor tolerances and in-batch processing variances.

Ionization data retrieval techniques were more reliable than the bridgewire technique. Thrust data acquisition and test arrangement need more development.

No significant permanent grain deformation was observed in the live-no-fire motors at 50- and 100-g acceleration loads. Any deformations that may have occurred were within the instrument measuring accuracy and original given tolerances.

References

[1] Thatcher, J. H., "Deformation of case bonded propellants under axial acceleration," Bulletin of the 20th Meeting of the Joint Army-Navy-Air Force Advanced Research Projects

Agency-NASA Panel on Physical Properties of Solid Propellants, Vol. I (1961).

[2] Chase, R. A. and Iwanciow, B. L., "Propellant slump in large solid propellant rocket motors during long-term vertical storage," Bulletin of the 20th Meeting of the Joint Army-Navy-Air Force Advanced Research Projects Agency-NASA Panel on Physical Properties of Solid Propellants, Vol. I (1961).

[3] Knauss, W. G., "Displacements in an axially accelerated solid propellant rocket grain," Bulletin of the 20th Meeting of the Joint Army-Navy-Air Force Advanced Research Projects Agency-NASA Panel on Physical Properties of Solid Propellants, Vol. I (1961).

[4] Williams, M. L., Blatz, P. J., and Schapery, R. A., "Fundamental studies relating to systems analysis of solid propellants," Graduate Astronautical Laboratory, California Institute of Technology, Final Rept. 101 (February 1961).

Approximation of Time of Ballistic Entry

Tom T. Kumagai*
North American Aviation, Inc., Anaheim, Calif.

Nomenclature

V = magnitude of the velocity vector, fps
γ = attitude of the velocity vector measured positively upward from the local horizontal (for entry trajectories, γ is always negative), deg
D = drag deceleration, $C_DA\ \rho V^2/2m$, ft/sec^2
g = gravitational acceleration, ft/sec^2
r = earth-centered radius vector, ft
ρ = density of the atmosphere, lb/ft^3
β = atmospheric decay coefficient, ft^{-1}
m = mass of the missile, lb
h = altitude, ft
W = weight of the missile, lb (used only in Fig. 1)

Introduction

MANY investigators have studied the segment of the entry trajectory in which the drag deceleration is large compared to the gravitational acceleration. One of the "classical" treatments under this restrictive condition is the one given by Allen and Eggers,[1] which is adequate for determining maximum deceleration and heating effects in the region of peak deceleration. It describes the air drag effects along a straight-line trajectory, since gravity is completely neglected. Moe[2] considers the gravity term in the equations of motion and by a transformation of variables determines an approximate trajectory representing the surface range as an integral solution. (As a special case, when $g = 0$, Moe's solution yields the Allen and Eggers solution.)

Figure 1 shows entry altitude and velocity characteristics for ballistic missiles with constant ballistic coefficients of 1000 and 1500 psf. The region in which gravity can be neglected, as in the Allen and Eggers approximation, is the portion of the trajectory below 90,000-ft alt, i.e., during the last 10 sec prior to impact. Neither Moe's nor Allen and Eggers' solution describes the effect of the air drag upon the entry time. This paper presents a useful method for approximating entry time, based upon the solution describing the exponential decay of the angular momentum on a zero-lift trajectory.

Received January 13, 1964; revision received June 17, 1964. This research is a part of Project DEFENDER, sponsored by the Advanced Research Project Agency, Department of Defense. The analysis was performed while the author was associated with Ground System Group, Hughes Aircraft Company, Fullerton, Calif. The author wishes to thank A. Darnell who checked the accuracy of the time predictor on the G-15 computer.

* Staff Scientist, Autonetics Division.

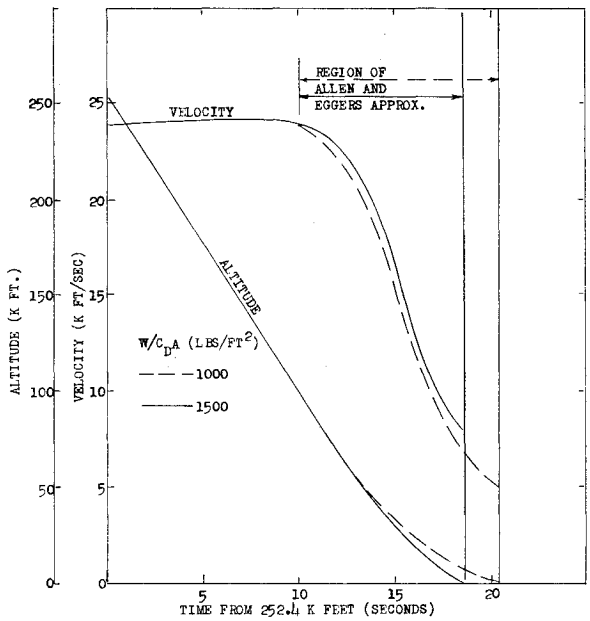

Fig. 1 Altitude and velocity vs time for constant W/C_DA (ballistic range: 5000 naut miles; entry angle: −40°).

Assumptions

The basic assumptions are that W/C_DA is constant and that the equations of motion can be expressed with the lift coefficients set equal to zero. The latter is reasonable for ballistic entry trajectories in which the arrow effect stabilizes the principle axis along the direction of the velocity vector, but it negates the admissibility of cross winds. In general, it can be assumed that ordinary winds and the windage caused by the rotating earth are small in comparison to the laminar flow about the re-entry vehicle caused by the shock wave front.

The atmosphere below 250,000 ft is represented by an exponential fit of the known atmospheric data.† The gravity vector is assumed to be represented by a simple inverse square field in the radius vector; neglecting the oblateness effect of the earth introduces insignificant errors.

A last assumption is that the local attitude angle of the missile's velocity vector with respect to its local horizontal is a slowly varying function and can be replaced by its mean value. For calculation purposes, the initial condition value is chosen instead of the mean value; this replacement introduces a significant error only for altitudes below 25,000 ft.

Decay of the Angular Momentum

In the case of a nonlifting trajectory, the equations of motion in the direction of the velocity vector and normal to the velocity vector are

$$\dot{V} = -g\sin\gamma - D \tag{1}$$

$$V\dot{\gamma} = (-g + V^2/r)\cos\gamma \tag{2}$$

Upon transforming Eq. (1) to the γ derivative, i.e.,

$$\dot{V} = \dot{\gamma}\, dV/d\gamma$$

where

$$\dot{\gamma} = [-(g/V) + (V/r)]\cos\gamma.$$

Eq. (1) becomes

$$\frac{1}{V}\frac{dV}{d\gamma} = \tan\gamma + \frac{D}{g\cos\gamma} + \frac{V}{gr}\frac{dV}{d\gamma} \tag{3}$$

† For some applications, a better curve fit can be obtained by dividing the atmosphere into spherical concentric shells, and curve fitting the exponential model atmosphere to each layer of atmosphere with a continuous transition at the boundaries of the concentric shells.